Publisher: Research Council of Science and Technology, Biratnagar, Nepal p.40

BIBECHANA

A Multidisciplinary Journal of Science, Technology and Mathematics

ISSN 2091-0762 (print), 2382-5340 (online)

Journal homepage: http://nepjol.info/index.php/BIBECHANA

Molecular electrostatic potential, HOMO-LUMO and vibrational study of aristolochic acid II using density functional theory

Jang Bahadur Khadka[1], Bhawani Datt Joshi[2*]

[1]Department of Chemistry, Siddhanath Sc. Campus, Mahendranagar, Tribhuvan University, Nepal

[2]Department of Physics, Siddhanath Sc. Campus, Mahendranagar, Tribhuvan University, Nepal

* E-mail: bdjoshi_007@yahoo.com

Accepted for publication: December 12, 2014

Abstract

Because of their wide applications in human or animal medicine, the natural products have been the subject of investigation. Aristolochic acids (AAs) (Aristolochiaceae), however toxic, are reported for many medicinal uses. In this work, computational study on the molecular properties of AA II is presented using density functional theory (DFT), B3LYP functional along with Hartree-Fock (HF) theory at 6-311++G(d,p) level. A complete vibrational assignment has been done for the observed FT-IR and Raman wavenumbers with the results of quantum chemical calculations. The structure–activity relationship has been interpreted by mapping electrostatic potential surface (MEP). Graphical representation of frontier molecular orbitals with their energy gap has been analyzed theoretically for both the gaseous and solvent environment employing TD-DFT using IEF-PCM model.

DOI: http://dx.doi.org/10.3126/bibechana.v12i0.11702

Keywords: MEP; HOMO-LUMO; vibrational spectroscopy; DFT.

1. Introduction

Medicinal plants play a fundamental role in the world health, since they are sources of several pharmacologically active compounds such as flavonoids and tannins. Many of these molecular structures are similar to those of our molecules and this is the basis for their physiological action [1]. The use of medicinal plants has been an elected practice throughout human history. It is important to point out that the plants, in addition to their therapeutic use in folk medicine, have contributed to the obtention of many drugs which are still in use, such as morphine, the main anesthetic alkaloid in opium, vincristine etc.

Aristolochic acids (AAs), found in *Aristolochia* spp, are structurally related nitrophenanthrene carboxylic acids. Drugs derived from *Aristolochia* plants have been used as medicine in obstetrics and in the treatment of snake bites [2]. The plant extracts have also been used for the therapy of arthritis, gout, rheumatism, and festering wounds [3,4]. However, aristolochic acid is an established human carcinogen [5,6], increase risk of developing urothelial carcinoma [7-11] in the patients with endemic nephropathy and chronic renal failure with some herbal medicines [12].

In this communication, we have presented molecular electrostatic potential surface (MEP), highest occupied molecular orbitals (HOMO)- lowest unoccupied molecular orbital (LUMO), and the vibrational spectra of the molecule aristolochic acid II (AA II) using *ab initio* Hartree-Fock (HF) and density functional theory (DFT). With the help of specific scaling procedures, the observed vibrational wavenumbers were analyzed and accurately assigned to different normal modes of the molecule; and using PED's the contributions of the different modes to each wavenumber were determined.

2. Methodology

2.1 Experimental

Infrared spectra were recorded on a Bruker TENSOR 27 FT-IR spectrometer with a spectral resolution of 4 cm^{-1} in the region 400-4000 cm^{-1}. KBr pellets of solid samples were prepared from mixtures of KBr and the sample in 200:1 ratio using a hydraulic press. Multi-tasking OPUS software was used for base line corrections.

The FT-Raman spectra were recorded on a Perkin-Elmer 2000R spectrometer as powder sealed in a capillary tube in the region 100-3500 cm^{-1}. The 1064 nm line of an Elforlight Model L04-2000S Nd: YAG laser was used as the exciting source with an output power of about 100 mW at the sample position. All spectra were accumulated for 100 scans with a resolution of 4 cm^{-1}.

2.2 Computational

Geometry optimization has been performed as the first task of the computational work. The geometric parameters available from the PubChem data base [13] have been used as the basis for the optimization. The molecular structure, vibrational frequencies and energies of the AA II were computed employing the DFT [14] method using Gaussian 09 program [15] package and Becke's three parameter (local, non-local, Hartree–Fock) hybrid exchange functional with Lee–Yang–Parr correlation functional (B3LYP) [16–18]. The split valence basis set 6-311++G(d,p), augmented by 'd' polarization functions on heavy atoms and 'p' polarization functions on hydrogen atoms as well as diffuse functions for both hydrogen and heavy atoms were used [19,20]. The IR absorption intensities and absolute Raman intensities were calculated in the same level of theory as used for the optimized geometry. The normal mode analysis was performed and the PED was calculated, employing GAR2PED program [21], along the internal coordinates using localized symmetry. For this purpose, a complete set of 90 internal coordinates were defined using Pulay's recommendations [22,23]. The vibrational assignments of the normal modes were done on the basis of the band profile, intensity and PED. Gauss-View program [24] was used for graphical presentation of the calculated Raman and IR spectra. To elucidate the differences of first excitation energies and oscillator strengths in gas and solution, the solvent effects were taken into account by means of integral equation formalism polarizable continuum model (IEF-PCM) [25-27].

3. Results and discussion

3.1 Geometry optimization

Geometry optimization has been performed as the first task in the *ab initio* calculations, using the molecular conformation obtained from PubChem data base [13]. The ground state optimized structure (in gas phase) of the molecule is presented in Fig. 1. The optimized parameters have been used for the other calculations. Some of the calculated bond parameters are listed below in the Table 1.

Table 1. Some calculated (DFT) bond parameters of AA II.

Bond length (Å)	Bond Angle (^{o})	Dihedral Angle (^{o})
C23-O4 = 1.2079	C13-C23-O3 = 112.74992	C17-C13-C23-O3 = 35.36312
O4-O6 = 2.87273	C12-C23-O4 = 124.70005	16-C13-C23-O4 = 30.81523
O4-O5 3.17938	C14-N7-O6 = 116.97323	C9-C14-N7-O6 = 34.44447
O6-H32 2.27952	C14-N7-O5 = 117.98883	C16-C14-N7-O5 = 38.83665
O1-H26 2.13096	O6-N7-O5 = 124.87079	C13-C23-O3-H32 = 176.71139

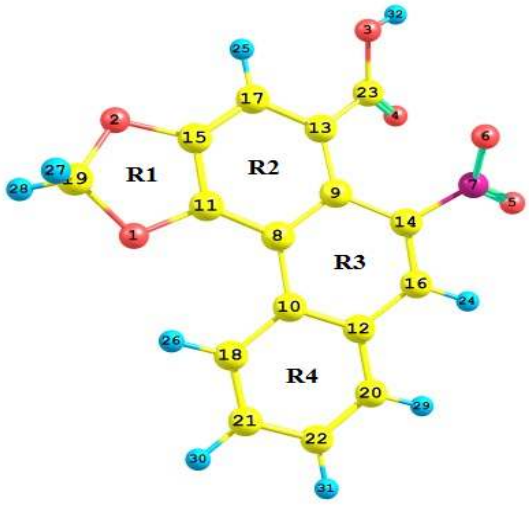

Fig. 1. Opitmized structure of AA II.

The equilibrium geometry has been determined by the energy minimization. The energy calculated by DFT (-1121.42720029 Hartree) is lower than the one calculated by HF (-1114.91828124 Hartree) as it should be. Similarly, the dipole moment calculated by DFT (6.6567 Debye) is higher than that calculated by HF (6.4607 Debye).

3.2 Molecular electrostatic potential

Molecular electrostatic potential surface is a good tool for assessing the reactive sites towards positively or negatively charged reactants to explain hydrogen bonding and structure-activity of the molecule; however, the molecular charge distribution remains unperturbed through the external test charge [28]. By quantum chemical calculations it is observed that there is a strong correlation between the dipole moment, electro-negativity, and partial charges with electrostatic potential [29]. It provides a visual method to understand the relative polarity of a molecule through mapping total density surface on electrostatic potential energy surface, which depict the size, shape, charge density, and site of chemical reactivity of the molecules.

.

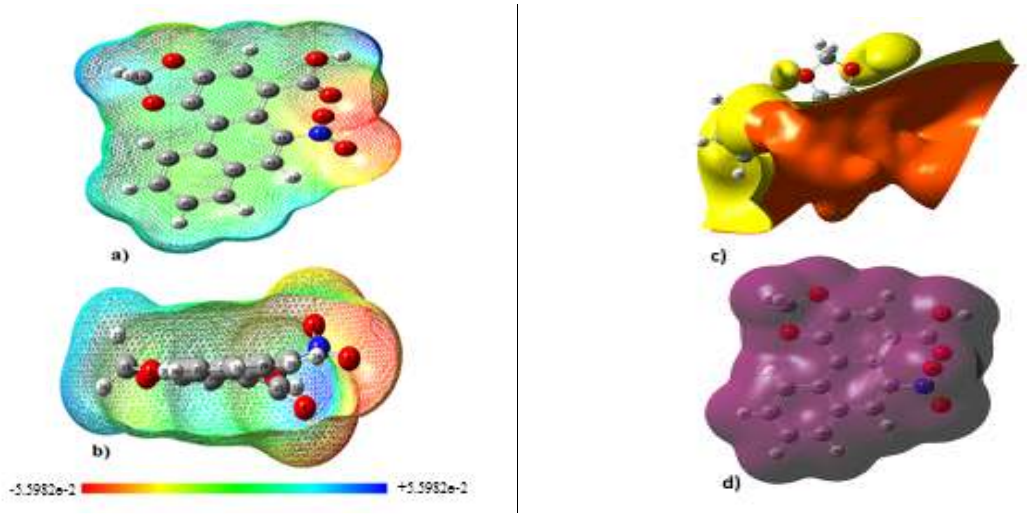

Fig. 2. (a & b) MEP (molecular electrostatic potential) (c) ESP (electrostatic potential), and (d) ED (Electron density) mapped on the isodensity surface from -5.5982 e-2 to +5.5982 e-2.

The MEP plots of AA II, shown in the Fig. 2, was based on the calculations performed with B3LYP/6-311++G(d,p) level of theory visualized with Gauss view program 5.0 [30]. In this molecule, regions near the oxygen atoms of methyl group are most negative (red regions) due the concentrated electron density. The regions near the hydrogen atoms of the same group are the most positive regions (blue regions) which correspond to the repulsion of proton by low electron density. The ED (electron density) plots of the investigated molecule show uniform charge distribution. However, yellowish blob from the ESP (electrostatic potential), in the Fig 2(c), reflects that the negative ESP is localized more over the oxygen atoms and the positive ESP is localized on the rest of the molecule. This result is expected, because ESP correlates with electro negativity and partial charges.

3.3 Frontier molecular orbitals and electronic absorption

The electronic transition corresponds from HOMO (characterizes of electron giving) to the LUMO (characterizes of electron accepting) orbital. Both the frontier molecular orbitals (FMOs), highest occupied molecular orbital (HOMO) and lowest unoccupied molecular orbital (LUMO) are the main orbitals taking part in chemical reaction. The electron delocalization between these orbitals is a principal factor in determining the easiness of a chemical reaction and the stereo-selective path, irrespective of intra and intermolecular processes. The energy gap between the HOMO and LUMO molecular orbitals characterizes the chemical reactivity and kinetic stability along with spectroscopic properties [31].

The electronic transitions of high oscillatory strength (f) along with their absorption wavelength (λ_{max}) and excitation energies (eV), obtained from the time dependent DFT (TD-DFT) calculation employing 6-31G(d,p) level of theory [32,33], have been listed in the Table 2.

The negative values of all the FMO energies indicate the stability of the title molecule. The calculation in the gas phase shows that the bands at 389.22, 269.69, 208.29 and 206.13 nm originate due to H→L, H-1→L+1, H-4→L+2 and H-7→L+1 transitions, respectively. However, the electronic transitions between these FMOs occur with some different values of λ and the oscillatory strengths. This discripancy is due to the solvent effect on the molecular orbitals. The HOMO-LUMO plot is shown below in the Fig. 3.

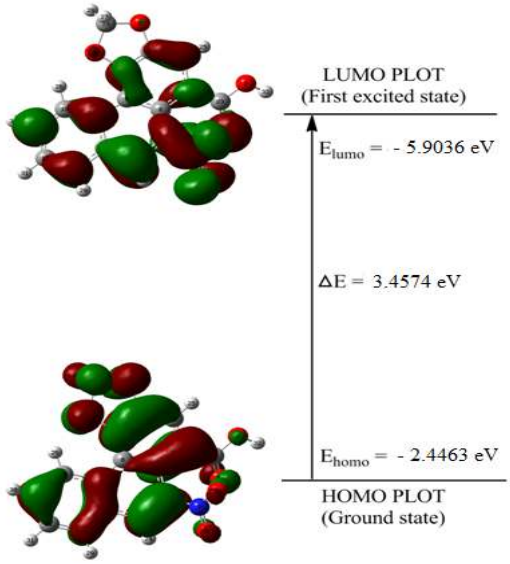

Fig. 3. HOMO-LUMO plot of AA II in the gas phase.

3.4 Vibrational wavenumbers

The total number of atoms in AA II molecule is 32 and gives 90 (3N-6; N- the number of atoms) normal modes of vibrations. All the fundamental modes of vibrations are both FT-IR and Raman active. As DFT calculation yields Raman scattering amplitude but not the Raman intensities, so the Raman scattering amplitudes can be predicted for each wavenumber using a relation [34,35];

$$\frac{\partial \sigma_j}{\partial \Omega} = \left(\frac{2^4 \pi^4}{45}\right) \left[\frac{\left(\nu_0 - \nu_j\right)^4}{1 - \exp\left[\frac{-hc\nu_j}{kT}\right]}\right] \left(\frac{h}{8\pi^2 c \nu_j}\right) S_j$$

where S_j and υ_j are the calculated scattering activities and the predicted wavenumbers, respectively, of the j^{th} normal mode, υ_0 is the Raman excitation wavenumber and h, c and k are the universal constants.

Table 2. Electronic transitions, absorption wavelength λ_{max} (nm), excitation energy (eV), oscillator strengths (f), frontier orbital energies (eV) and dipole moment (Debye).

Excited states	Gas phase				Solvent phase				Transition types
	Transition states	λ_{max}	E (eV)	Oscilator strength (f)	Transition states	λ_{max}	E (eV)	Oscilator strength (f)	
1	H→L	389.22	3.1855	0.0538	H→L	428.20	2.8955	0.0559	$\pi\rightarrow\pi^*$
2	H-1→L	337.82	3.6701	0.0028	H-1→L	355.67	3.4859	0.0046	$\pi\rightarrow\pi^*$
3	H-2→L	331.52	3.7399	0.0104	H→L+1	340.88	3.6372	0.1354	$\pi\rightarrow\pi^*$
4	H→L+1	325.78	3.8058	0.0939	H-2→L	321.46	3.8569	0.1008	$\pi\rightarrow\pi^*$
5	H→L+2	304.96	4.0656	0.0894	H→L+2	318.42	3.8937	0.0732	$\pi\rightarrow\pi^*$
6	H-1→L+1	269.69	4.5973	0.1155	H-1→L+1	281.14	4.4101	0.0905	$\pi\rightarrow\pi^*$
7	H-3→L+1	261.71	4.7374	0.1583	H-1→L+1	275.03	4.5081	0.1723	$\pi\rightarrow\pi^*$
8	H-1→L+1	252.87	4.9031	0.1294	H-2→L+1	265.17	4.6756	0.0637	$\pi\rightarrow\pi^*$
9	H→L+3	245.47	5.0509	0.0615	H-1→L+2	259.49	4.7780	0.2527	$\pi\rightarrow\pi^*$
10	H-4→L+1	237.32	5.2244	0.1899	H-1→L+2	242.99	5.1024	0.3188	$\pi\rightarrow\pi^*$
11	H→L+5	222.51	5.5721	0.1024	H→L+4	229.71	5.3974	0.0620	$\pi\rightarrow\pi^*$
12	H-8→L	217.15	5.7097	0.0719	H-4→L+1	221.30	5.6025	0.2128	$\sigma\rightarrow\pi^*$
13	H-4→L+2	208.21	5.9548	0.2432	H-1→L+3	215.89	5.7429	0.2100	$\sigma\rightarrow\pi^*$
14	H-7→L+1	206.13	6.0149	0.2034	H-3→L+2	212.62	5.8313	0.057	$\sigma\rightarrow\pi^*$
15	H-8→L+1	200.22	6.1923	0.0838	H-2→L+3	201.04	6.1672	0.1219	$\sigma\rightarrow\pi^*$

	E_{HOMO} (eV)	E_{LUMO} (eV)	ΔE (eV)	μ (D)
Gas	- 5.90364486	- 2.44626063	3.45738423	6.9762
Ethanol	- 5.90359044	- 2.44103631	3.46255413	8.1606

The calculated Raman and IR intensities were used to convolute each predicted vibrational mode with a Lorentzian line shape (FWHM = 8 cm^{-1}) to produce simulated spectra. Since, the DFT and HF vibrational wavenumbers are known to be higher than the experimental wavenumbers due to neglect of anharmonicity effects, they were scaled down by the wavenumber linear scaling procedure (WLS) [υ_{obs} = (1.0087–0.0000163 υ_{calc}) υ_{calc} cm^{-1}] of Yoshida et al. [36]. Comparison of the wavenumbers, calculated with the HF and DFT method with experimental values, reveals that the DFT method shows very good agreement with experimental observation than the HF due to inclusion of electron correlation, approximate treatment of basis set deficiencies and for the anharmonicity.

The detailed comparison of observed and scaled wavenumbers along with the potential energy distribution is presented in Table 3. The comparison of observed and calculated FT-IR and Raman spectra of AA II molecule is presented in Figs. 4 and 5, respectively. The description of vibrational assignments of the 4 rings and the functional groups has been given below:

3.4.1 O-H vibrations

In this molecule, there is one hydroxyl group (O-H) attached at the ring R2 through carbonyl. The hydroxyl group vibrations are the most sensitive to the environment, so the hydrogen bonded species show pronounced variation in the observables of a spectral band, such as band intensity and shape, frequency position of band maxima. The free hydroxyl group absorbs strongly in the region 3600–3550 cm^{-1}, whereas the existence of hydrogen bond can

lower the O-H stretching wavenumber to the 3550–3200 cm^{-1} region with an increase in IR intensity and breadth [37]. In our study, the O-H stretching is calculated at 3566/3875 cm^{-1} in scaled DFT/HF and match with very weak band at 3477 cm^{-1} in the IR spectrum, which indicates the group involvement in intermolecular hydrogen bonding. The O-H deformation is calculated at 1164/1245 cm^{-1} in the DFT/HF and assigned to the observed peaks at 1149/1148 cm^{-1} in the IR/Raman spectra.

3.4.2 C=O vibrations

Most of the characteristic features of the carboxylic group are observed usually 1750–1600 cm^{-1} region [38]. C=O bonds being highly polar show intense peak in the IR and weak peak the Raman spectra. The C=O stretching vibration is calculated at 1749 cm^{-1}, which match with the observed strong peak at 1687 cm^{-1} in the IR and weak peak at 1740 cm^{-1} in the Raman spectra, respectively. The wagging, deformation and rocking of C=O are calculated at 800/889, 665/721 and 431/464 cm^{-1} in the DFT/HF showing good agreements with the observed wavenumbers at 791/797, 650/672 and 420/430 cm^{-1} in the IR/Raman spectra.

Table 3. Observed and calculated FT-IR and Raman wavenumbers (cm^{-1}) of AA II.

Un-scaled DFT	Scaled DFT	HF	Observed IR	Raman	PED %
3765	3566	3875	3477	-	υ(OH)(100)
3250	3106	3269	3097	3096	R4[υ(CH)](98)
3229	3087	3233	3078	3083	R2[υ(CH)](99)
3204	3065	3223	-	3072	R3[υ(CH)](99)
3192	3054	3199	3020	3042	R4[υ(CH)](99)
3177	3040	3184	3018	3032	R4[υ(CH)](99)
3169	3032	3175	3016	3028	R4[υ(CH)](99)
3131	2998	3160	2999	2997	R1[$\upsilon_a(CH_2)$](99)
3012	2890	3061	2852	2880	R1[$\upsilon_s(CH_2)$](100)
1785	1749	1933	1687	1740	υ(C=O)(77)+R2[υ(C13C23)](6)
1660	1630	1804	1685	1624	R3[υ(CC)(40)+δ_a(10)+δ_{in}(CH)(5)]+R2[υ(CC)](9)+R1[υ(CC)](7)
1648	1618	1761	1626	1609	R4[υ(CC)(51)+δ_a(8)+δ_{in}(CH)(12)]
1630	1600	1755	1595	1593	R2[υ(CC)(26)+δ_a(6)]+R1[υ(CC)](21)+R4[υ(CC)](12)+R3[υ(CC)](7)
1620	1591	1740	1593	1591	R2[υ(CC)(46)+δ'_a(9)+δ_{in}(CH)(6)]+R1[δ'_{ring}](6)+R3[υ(CC)](5)
1589	1562	1734	1539	1543	$\upsilon_a(NO_2)$(78)+$\rho(NO_2)$(6)
1569	1543	1678	1525	1541	R4[υ(CC)(30)+δ_{in}(CH)(10)]+R3[υ(CC)](22)+R2[υ(CC)](6)
1539	1514	1648	1523	1508	R1[$\delta(CH_2)$](77)
1529	1504	1630	1506	1507	R4[δ_{in}(CH)(23)+υ(CC)(5)]+R3[υ(CC)](23+R1[δ(CH2)](17)
1480	1458	1603	1452	1451	R4[δ_{in}(CH)(31)+υ(CC)(16)]+R3[υ(CC)(8)+δ_{trig}](7)]+R2[υ(CC)](14)
1473	1450	1581	1450	1449	R2[υ(CC)(20)+δ_{in}(CH)(7)]+R4[δ_{in}(CH)](15)+υ(CC)(8)]+R3[υ(CC)](15)+ R1[υ(CO)](7)
1436	1415	1569	1417	1406	R1[$\omega(CH_2)$](42)+R3[υ(CC)](11)+δ_{in}(CH)(5)]+R2[δ_{trig}](8)
1422	1401	1543	-	1391	R1[$\omega(CH_2)$](30)+R3[υ(CC)(16)+δ_{in}(CH)(11)]+R4[δ_{in}(CH)](10)
1400	1380	1516	1373	1372	R2[υ(CC)(33)+υ(C13C23)(12)]+R1[υ(CO)](14)
1377	1358	1502	1350	1350	R2[υ(CC)(21)+δ_{in}(C13C23)(6)]+R3[υ(CC)](25)
1371	1353	1473	1348	1348	$\upsilon_s(NO_2)$(57)+$\delta(NO_2)$(14)+R3[υ(CN)](12)
1360	1342	1416		1347	R4[υ(CC)](44)+R3[υ(CC)](11)+R3[δ_{in}(CH)](9)
1350	1332	1387	1331	1331	R2[υ(CC)](37)+R1[υ(CC)](10)+R3[υ(CC)](8)+δ(CHO)(5)
1321	1304	1376	-	-	R4[δ_{in}(CH)](17)+υ(CC)(5)]+R3[υ(CC)](11)+δ_{trig}(6)]+δ(CHO)(14)+R2[υ(CC)](8)
1287	1271	1344	1273	1271	R4[δ_{in}(CH)(19)+υ(CC)(10)]+R2[υ(CC)(16)+δ_{in}(CH)(9)]+R3[υ(CC)(11)+δ_{trig}(5)]
1269	1253	1328	1348	1246	R4[υ(CC)(14)+δ_{trig})(10)+δ_{in}(CH)(9)]+R3[υ(CC)](27)+R1[υ(CO)](8)
1231	1217	1322	-	1213	R1[$\gamma(CH_2)$(9)+υ(CO)(9)]+R3[δ_{in}(CH)](17)+R2[δ_{trig}(9)+δ_{in}(CH)(7)]+R4[υ(CC)](9)+δ(CHO)(5)
1220	1206	1302	1205	1194	R1[$\gamma(CH_2)$](77)
1202	1189	1282	1171	1173	R2[δ_{in}(CH)(29)+υ(CC)(13)]+R3[δ_{in}(CH)(12)+υ(CC)(10)]+R4[δ_{in}(CH)](7)
1195	1182	1266	1169	1171	R4[δ_{in}(CH)(49)+υ(CC)(8)]+δ(CHO)(8)+R2[δ_{in}(CH)](6)
1177	1165	1244	1149	1148	δ(OH)(20)+υ(CO)(18)+R4[δ_{in}(CH)](14)+R2[υ(C13C23)](7)
1160	1148	1234	1147	1142	R4[δ_{in}(CH)(30)+υ(CC)(17)]+R3[δ_{trig}](9)+R4[δ_{trig})](7)
1146	1134	1223	1126	1115	R1[$\rho(CH_2)$](85)
1122	1111	1175	1080	1113	υ(CO)(20)+R2[δ_{trig}](18)+R1[υ(CO)](17)+δ(CHO)(5)
1076	1067	1171	1066	1067	R1[υ(CO)](33)+R3[υ(CN)(7)+δ_{trig}(5)]+R4[δ_{trig})](7)

1065	1056	1149	1065	1065	R4[υ(CC)(52)+δ_{in}(CH)(9)]+R1[υ(CO)](16)
1053	1044	1109	1043	1040	R1[υ(CO)](32)]+R4[υ(CC)](10)+R2[υ(CC)](9)+R3[υ(CN)](8)
1005	997	1107	999	1001	R4[oop(CH)(86)+puck(11)]
987	980	1104	982	980	R1[υ(CO)](25)+R2[δ'_a(10)+υ(C13C23)(7)+δ_{trig}(5)]+R3[δ_{trig}(14)+υ(CN)(7)]+R4[δ_{trig})](11)
980	973	1084	962	9961	R4[oop(CH)](89)+R4[τ'_a](5)
952	946	1065	943	947	R1[υ(CO)](68)+R1[δ'_{ring}](8)
933	927	1043	920	928	R3[oop(CH)](63)+ puck(12)+oop(CN)(7)]
925	919	1011	903	915	R4[δ_{trig})](30)+R1[ν(CO)](14)+R3[υ(CN)](8)+δ(NO_2)(7)+R2[δ_a](6)
905	899	997	901	897	R2[oop(CH)(73)+oop(C13C23)(6)+puck(7)+τ_a(6)]
881	876	970	877	872	R4[oop(CH)(81)+puck(5)]
870	865	934	856	862	R3[υ(CC)(23)+δ'_a(6)]+R4[υ(CC)](10)+δ_{trig})(5)]+R1[υ(CO)(10)+υ(CC)(5)]+R2[δ_a](8)
846	842	915	841	839	δ(NO_2)(30)+R3[υ(CC)(6)+δ_a(5)]+R2[υ(C13C23)](9)+R4[δ_{trig})](8)
804	800	889	791	797	ω(C=O)(30)+R2[oop(15)+δ_{in})(6)](C13C23)(6)+puck(5)]+R1[δ_{ring}](6
790	787	880	789	780	R3[puck](16)+R2[puck(14)+oop(C13C23)(11)]+R1[δ_{ring}](12)+ω(C=O)(7)
787	784	860	777	778	R3[oop(CN)(15)+puck(15)]+ω(NO_2)(15)+R4[oop(CH)](15)+R2[puck](13)
775	772	856	766	770	R4[puck](37)+R3[puck](22)+ω(NO_2)(7)+R2[τ_a](5)
766	763	840	754	756	R4[oop(CH)](51)+R3[puck(11)+oop(CN)(7)]+R2[puck](7)
751	748	818	729	745	R1[δ'_{ring}(31)+δ_{ring}(24)]+R1[υ(CO)](7)
735	733	806	727	726	R2[puck(24)+τ_a(8)]+R4[puck](16)+R3[δ'_a](6)
721	719	784	714	-	R2[puck](36)+R4[puck](6)+R1[δ'_{ring}](5)
702	700	765	700	702	R2[τ'_a(10)+oop(C13C23)(7)+δ_{in}(C13C23)(7)+ω(NO_2)(7)
687	685	750	675	683	R2[τ'_a](25)+R3[oop(CN)(9)+puck(7)]+τ(C8C9)(9)+R1[τ](5)
667	665	721	650	672	R4[δ_a)](32)+δ[(C=O)](22)
623	622	672	621	619	R4[δ'_a)(30)+δ_a)(8)]+δ(C=O)](16)+R2[δ_a](8)
617	616	662	619	618	τ(O3C23)(23)+R2[oop(C13C23)(17)+τ_a(6)+puck(5)]+R3[puck(7)
609	608	659	607	600	R4[puck](12)+R4[δ'_a)](12)+δ_a(8)]+R2[τ_a](11)+R3[puck](10)
584	583	628	592	589	τ(O3C23)(16)+R3[δ_a(11)+oop(CN)(5)]+R2[τ'a](11)+τ(C10C12)(5)
543	543	587	550	537	R2[τ'_a(20)+τ_a(10)]+R3[oop(CN)(11)+puck(11)]+R4[τ'_a](12)
536	536	580	530	531	R2[τ'_a(10)+δ'_a(9)+puck(5)+R3[δ_a](10)+ρ(NO_2)(9)+τ(C8C9)(7)+τ(C10C12)(6)+ρ(C=O)(6)
512	512	557	507	504	R2[τ_a(24)+oop(C13C23)(9)]+R3[oop(CN)](11)+R4[τ_a(10)+τ'_a(8)]
450	450	493	447	447	R4[τ'_a(24)+τ_a(18)]+R2[τ_a](16)+τ(C10C12)(11)+τ(C11C15)(6)
431	431	464	420	430	R2[δ'_a(13)+τ_a(9)]+R3[oop(CN)(6)+δ'_a(6)]+ρ(C=O)(10)+τ(C11C15)(7)+R2[puck](7)
401	402	436	-	402	R3[δ_a](14)+ρ(NO_2)(13)+R4[τ'_a](13)+R2[δ_a](10)+τ(C11C15)(5)
375	376	409	-	378	R2[τ'_a(15)+δ'_a(10)]+τ(C11C15)(14)+R4[τ'_a](13)+ρ(N=O)(8)
353	354	376	-	346	R2[δ_a(15)+δ'_a(14)+υ(CC)(7)]+R3[δ'_a(25)+δ_a(5)]+R1[υ(CO)](5)
339	340	366	-	344	R3[υ(CN)(21)+υ(CC)(13)+δ'_a(11)]+R2[υ(CC)(10)+υ(C13C23)(7)]+δ[(C=O)](5)
328	329	361	-	-	R2[oop(C13C23)(13)+τ'_a(9)+τ_a(8)]+τ(C8C9)(12)+R1[τ](11+τ(C11C15)(9)+R2[puck](5) +ρ[(C=O)](5)
302	303	330	-	308	τ(C11C15)(33)+R2[τ_a(6)+τ'_a(6)]+R4[τ_a](9)+R1[τ'](7)+R3[puck](6)
274	275	299	-	288	τ(C11C15)(13)+R3[δ_a](9)+τ(C8C9)(6)+R4[τ'_a](8)
257	259	283	-	255	R3[oop(CN)](30)+R4[τ'_a](16)+R2[τ_a](11)+τ(C8C9)(5)
203	204	222	-	201	R2[τ'_a(16)+oop(C13C23)(8)]+R3[δ_{in}(CN)](15)+R1[τ](13)+τ(C10C12)(12)+R4[τ_a](7)
198	199	213	-	199	R2[δ_{in}(C13C23)(17)+oop(C13C23)(7)+τ'_a(6)]+R1[τ](11)
185	186	204	-	-	R2[oop(C13C23)(17)+τ'_a(15)]+τ(C10C12)(14)+R4[τ_a](9)+R1[τ](6)+R3[oop(CN)](5) +τ(C11C15)(5)
173	174	188	-	-	R2[δ_{in}(C13C23)(19)+τ'_a(7)]+R3[δ_{in}(CN)](17)+τ(C10C12)(13)+R4[τ_a](7)+R1[τ'](5)
154	155	164	-	151	R1[τ'(50)+τ(27)]
109	109	124	-	-	τ(NC)(37)+R2[δ_{in}(C13C23)(14)+τ'_a(5)]+R3[δ_{in}(CN)](9)
100	101	111	-	-	R2[τ'_a(25)+τ_a(12)]+τ(C11C15)(13)+R1[τ](10)+τ(NC)(9)+τ(C10C12)(8)
92	93	100	-	85	R2[oop(C13C23)](19)+τ(C8C9)(16)+R3[oop(CN)](14)+R1[τ'](12)+τ(C10C12)(9)+R1[τ](7)
80	81	90	-	83	τ(NC)(31)+τ(C13C23)(30)+R2[τ_a(11)+τ'_a(5)]+τ(C10C12)(8)
69	69	76	-	-	R2[τ'_a(39)+τ_a(10)]+τ(C13C23)(12)+τ(C8C9)(10)+τ(C10C12)(8)+R4[τ_a](8)
38	38	41	-	41	R2[τ_a(27)+τ'_a(11)]+τ(C13C23)(20)+τ(C8C9)(20)+τ(NC)(7)

Proposed assignments and potential energy distribution (PED) for vibrational normal modes.
Types of vibration: ν, stretching; δ, deformation (bending), scissoring; oop, out-of-plane bending; ω, wagging; γ, twisting; ρ, rocking; τ, torsion.
[a]Potential energy distribution (contribution ≥ 5).

3.4.3 C-NO_2 vibrations

There is one nitro (NO_2) group connected with the ring R3 as a functional group in this molecule. Generally, the asymmetric NO_2 stretching modes are expected in the interval 1600-1500 cm^{-1} and symmetric stretching modes in the interval 1400–1300 cm^{-1} in the IR absorption bands [39]. In this study, the asymmetric N=O vibration is calculated at 1562/1734 cm^{-1} in the DFT/HF, which matches well with a weak band at 1539 cm^{-1} in the IR and the medium intensity band at 1534 cm^{-1} in the Raman spectrum.

cm^{-1} in the Raman spectrum. The symmetric N=O vibration is calculated at 1353/1473 cm^{-1} in the DFT/HF, which is observed with the weak intensity at 1348 cm^{-1} in the IR spectrum and the strong peak at 1348 cm^{-1} in the Raman spectrum. This mode is mixed with NO_2 deformation and C-N stretching vibration of the ring. The deformation (or scissoring) of NO_2 vibration is calculated at 842/915 cm^{-1} in the DFT/HF and observed at 841/839 cm^{-1} in the IR/Raman spectra. The NO_2 wagging vibration is calculated at 784/860 in DFT/HF, which is observed at 777 cm^{-1} in the IR spectrum and 778 cm^{-1} in the Raman spectrum. The mixed rocking mode vibration of NO_2 is calculated at 536/580 cm^{-1} in DFT/HF.

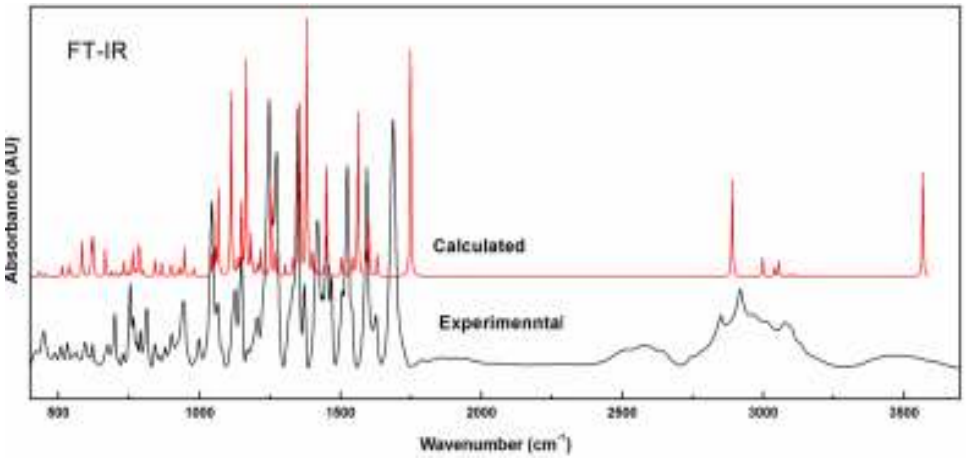

Fig. 4. Observed and calculated FT-IR spectra between the ranges 400-3600 cm^{-1}.

3.4.4 Ring R1 vibrations

There is one CH_2 moiety in this five membered planer ring. Basically, one can expect six fundamental modes associated with each CH_2 group vibrations namely: symmetric, asymmetric stretch, deformation and rocking modes which belong to polarized in-plane vibrations. In addition to that, CH_2 wagging and twisting modes would be expected to be depolarized out-of-plane symmetry species. The asymmetric CH_2 stretching vibrations are generally observed in the range 3000–2900 cm^{-1}, while the symmetric stretch appears in the region 2900–2800 cm^{-1} [40,41]. In this study, the pure CH_2 asymmetric stretching vibration is calculated at 2998/3160 cm^{-1} in the DFT/HF, which is observed at 2999 cm^{-1} in the IR spectrum and 2995 cm^{-1} in the Raman spectrum. Symmetric stretching vibrarion of this group is calculated at 2830/3061 cm^{-1} in the DFT/HF and assigned at 2852 cm^{-1} in the IR and 2880 cm^{-1} in the Raman spectra, respectively. The CH_2 deformation calculated at 1514/1648 cm^{-1} in the DFT/HF is observed with good agreements with strong band at 1523 cm^{-1} in the IR and with weak band at 1508 cm^{-1} in the Raman spectra, respectively. The mixed CH_2 wagging vibration is calculated at 1415/1569 cm^{-1} in the DFT/HF, which is assigned at 1417 cm^{-1} in the IR spectrum and at 1406 cm^{-1} in the Raman spectrum. The pure CH_2 rocking mode is calculated at 1134/1223 cm^{-1} in the DFT/HF. This mode is observed at 1126 cm^{-1} in the IR and at 1115 cm^{-1} in the Raman spectra, respectively. The twisting vibration of CH_2 is calculated at 1206/1302 cm^{-1} in the DFT/HF.

3.4.5 Ring R2 vibrations

An aromatic six membered ring R2 lying between R1 and R3 have a methine (CH) and a carboxyl (COOH) moiety as functional groups. The characteristic region for the identification of C-H stretching in the heteroaromatic structures is 3100–3000 cm^{-1} [42,43]. In this study, the C-H stretching vibration is calculated at 3087/3233 cm^{-1} in the DFT/HF as a pure mode. The observed IR/Raman peaks are at 3038/3083 cm^{-1}. The mixed in-plane deformation is calculated at 1189 in DFT and at 1282 cm^{-1} in HF, respectively. The observed wavenumbers of this mode are 1171 cm^{-1} in the IR spectrum and at 1173 cm^{-1} in the Raman spectrum. The C-H out-of-plane deformation is calculated at 899/997 cm^{-1} in the DFT/HF, which is observed at the peaks 901 cm^{-1} in the IR and at 897 cm^{-1} in the Raman spectra, respectively.

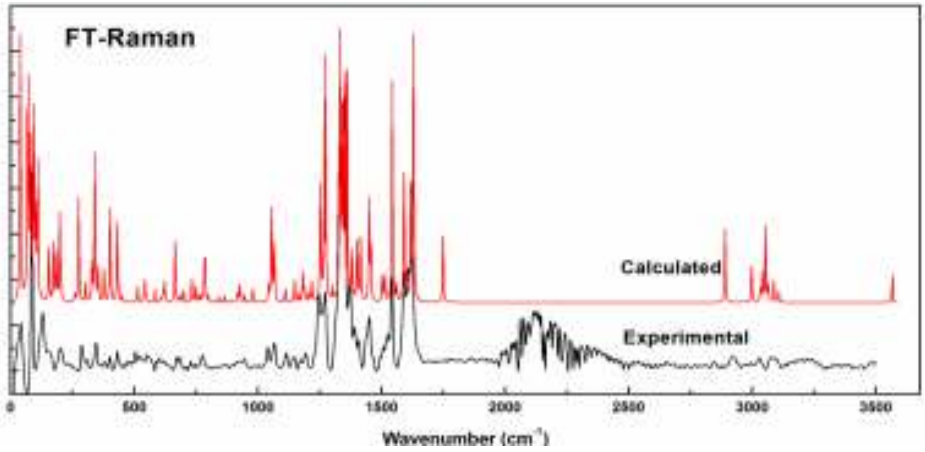

Fig. 5. Observed and calculated FT-Raman spectra between the range 0-3700 cm^{-1}.

3.4.6 Ring R3 vibrations

The six membered ring R3 has a CH and one NO_2 moiety. The C-H stretching vibration is calculated at 3065/3223 cm^{-1} in the DFT/HF and observed at 3072 cm^{-1} in the Raman spectrum. The C-H in-plane deformation is calculated at 1217/1322 cm^{-1} in DFT/HF and observed at the very weak band in Raman spectrum. The out-of-plane deformation is calculated at 927/1043 cm^{-1} in the DFT/HF, which is observed in the bands at 920 cm^{-1} in the IR and at 928 cm^{-1} in the Raman spectrum, respectively. The mixed C-C ring stretching vibrations are calculated below 772/856 cm^{-1} in the DFT/HF calculations. The highly mixed C-N stretching vibrations are calculated below 1380 cm^{-1} in DFT with low contributions. The DFT calculation yields C-N out-of plane deformations below 950 cm^{-1} as mixed modes and with low contributions. Similarly, the C-N and in-plane deformations are calculated below 500 cm^{-1}.

3.4.7 Ring R4 vibrations

Ring R4 is also a phenyl ring having four methine moieties and connected with the other ring R3 as shown in the Fig. 1. The C-H stretching vibrations are calculated as the pure modes in the ranges 3106-3032 in the DFT and 3269-3175 cm^{-1} in the HF, respectively. The mixed C-H in-plane deformations are calculated at 1504, 1528, 1271, 1182 and 1148 cm^{-1} in the DFT, which have good agreements with the observed IR and Raman bands. Similarly, these wavenumbers are calculated at 1630, 1603, 1344, 1266 and 1264 cm^{-1} in the HF method. The C-H out-of-plane deformations are calculated below 1000 cm^{-1} in the DFT. These mixed modes of vibration are calculated below 1110 cm^{-1} in the HF.

In the DFT, the C-C ring stretching vibrations are calculated at 1618 and 1543 cm^{-1}, which match with the strong peak at 1626, 1525 cm^{-1} in the IR spectrum and with the weak peaks at 1609, 1541 cm^{-1} in the Raman spectrum. The trigonal deformation, puckering, asymmetric deformation and asymmetric torsion of this ring are calculated at 919, 772, 622 and 450 cm^{-1} in the DFT method.

4 Conclusion

In the present study, the frequency assignments of the normal modes of AA II using the spectroscopic intuition as well as the quantum chemical calculations were performed. The comparison of the results of experimental and theoretical study has given a full description of the geometry, vibrational wavenumbers and electronic properties of this molecule. The scaled wavenumbers obtained using DFT/HF methods for AA II, showed good correlation with the observed Raman and FT-IR spectra. Any discrepancies noted between the observed and the calculated wavenumbers was observed due to the fact that the calculations have been actually performed on single (or isolated) molecule in the gaseous state. By mapping molecular electrostatic potential surface (MEP) on the electron density isosurface helps in assessing information regarding the size, shape, charge density distribution and sites of chemical reactivity of the title molecule. Our studies have shown that the DFT calculations are qualitative tools for assigning overall understanding of the electronic, structural and vibrational properties of the natural products.

Acknowledgements

The authors are grateful to Prof. Poonam Tandon, University of Lucknow, India for her suggestions and providing facility of the Gaussian 09 calculations.

References

[1] A.M. Soares, F.K. Ticli, S. Marcussi, M.V. Lourenço, A.H. Januário, S.V. Sampaio, J.R. Giglio, B. Lomonte and P. S. Pereira, Current Med. Chem., 12 (2005) 2625. http://dx.doi.org/10.2174/092986705774370655

[2] P. Balachandran, F. Wei, R.C. Lin, I.A. Khan and D.S Pasco, Kidney International, 67 (2005) 1797. http://dx.doi/10.1111/j.1523-1755.2005.00277.x

[3] V.G. Rucker and B.S. Chung, Planta. Med., 27 (1975) 68. http://dx.doi.org/10.1055/s-0028-1097762

[4] H.A. Priestap, Phytochemistry, 26 (1987) 519. http://dx.doi.org/10.1016/S0031-9422(00)81447-8

[5] V.M. Arlt, M Stiborova and H.H. Schmeiser, Mutagenesis, 17 (2002) 265. http://dx.doi.org/10.1093/mutage/17.4.265

[6] IARC Monographs on the evaluation of carcinogenic risks to humans: Some traditional herbal medicines, some mycotoxins, naphthalene and styrene, Volume 82. World Health Organization, International Agency for Research on Cancer (2002).

[7] I.N. Chernozemsky, I.S. Stoyanov, T.K. Petkova-Bocharova, I.G. Nicolov, I.V. Draganov, I.I. Stoichev, et al., Bulgaria. Int. J. Cancer., 19 (1977) 1 http://dx.doi.org/10.1002/ijc.2910190102.

[8] K. Sekar, S. Vaijayanthi Mala, M. Yogavel, D. Velmurugan, M.J. Poi, B.S. Vishwanath, T.V. Gowda, A.A. Jeyaprakash and M.D. Tsai, J. Mol. Biol. 333 (2003) 367. http://dx.doi/10.1016/j.jmb.2003.08.032

[9] S. Čeović and M. Miletić-Medved, Epidemiological features of endemic nephropathy in the focal area of Brodska Posavina, Croatia. In: D. Čeović, S. Čeović, A. Stavljenić-Rukavina, editors. Endemic nephropathy in Croatia. Zagreb: Academia Croatica Scientiarum Medicarum (1996) pp 7.

[10] V. Petronić, Tumors of the upper urothelium and endemic nephropathy. In: Z. Radovanović, M. Sindjić, M. Polenaković, L.J. Djukanović, V. Petronić, editors. Endemic nephropathy. Belgrade: Zavod za ud-benike inastavna sredstva (2000) pp 350-439.

[11] J. Gardiner, Z. Andreeva, D. Barton, A. Ritchie, R. Overall and J. Marc, Plant Biology 10 (2008) 725. http://dx.doi/10.1111/j.1438-8677.2008.00090.x

[12] S.Attaluri, R.R. Bonala, I.Y. Yang, M.A. Lukin, Y. Wen, A.P. Grollman, M. Moriya, C. R. Iden and F.Johnson, Nucleic Acids Research, 38 (2010) 339. http://dx.doi.org/10.1093/nar/gkp815

[13] www.ncbi.nlm.nih.gov Structure search data base.

[14] P. Hohenberg and W. Kohn, Phys. Rev. 136B (1964) 864. http://dx.doi.org/10.1103/PhysRev.136.B864

[15] M.J. Frisch et al., GAUSSIAN 09, Revision, Gaussian, Inc., Wallingford CT, 2009.

[16] C.T. Lee, W.T. Yang and R.G. Parr, Phys. Rev., 37 (1998) 785. http://dx.doi.org/10.1103/PhysRevB.37.785

[17] A.D. Becke, J. Chem. Phys., 98 (1993) 5648. http://dx.doi.org/10.1063/1.464913

[18] R.G. Parr and W. Yang, Density Functional Theory of Atoms and Molecules, Oxford, New York, 1989.

[19] G.A. Petersson, A. Bennett, T.G. Tensfeldt, M.A. Allaham, W.A. Shirley and J. Mantzaris, J. Chem. Phys., 89 (1988) 2193. http://dx.doi.org/10.1063/1.455064

[20] G.A. Petersson and M.A. Allaham, J. Chem. Phys., 94 (1991) 6081. http://dx.doi.org/10.1063/1.460447

[21] J.M.L. Martin and C. Van Aslenoy, Gar2ped, University of Antwerp, 1995. http://dx.doi.org/10.1021/ja00504a009

[22] P. Pulay, G. Fogarasi, F. Pang and J.E. Boggs, J. Am. Chem. Soc., 101 (1979) 2550. http://dx.doi/abs/10.1021/ja00504a009

[23] G. Fogarasi, X. Zhou, P.W. Taylor and P. Pulay, J. Am. Chem. Soc., 114 (1992) 8191. http://dx.doi.org/10.1021/ja00047a032

[24] A. Frisch, A.B. Nielson and A.J. Holder, Gauss View User Manual, Gaussian Inc, Pittsburgh, P.A., 2000.

[25] S. Miertuš, E. Scrocc and J. Tomasi, Chem. Phys., 55 (1981) 117. http://dx.doi.org/10.1016/0301-0104(81)85090-2

[26] S. Miertus and J. Tomasi, Chem. Phys., 65 (1982) 239. http://dx.doi.org/10.1016/0301-0104(82)85072-6

[27] M. Cossi, V. Barone, R. Cammi and J. Tomasi, Chem. Phys. Lett., 255 (1996) 327. http://dx.doi.org/10.1016/0009-2614(96)00349-1

[28] B.D. Joshi, R. Mishra, P. Tandon, A. C. Oliveira and A. P. Ayala, J. Mol. Struct., 1058 (2014) 31. http://dx.doi.org/10.1016/j.molstruc.2013.10.062

[29] C. Muňoz-Caro, A. Niňo, M.L. Sement, J.M. Leal and S. Ibeas, J. Org. Chem., 65 (2000) 405. http://dx.doi.org/10.1021/jo991251x

[30] A. Frisch, A.B. Nielson and A.J. Holder, GaussView User Manual, Gaussian Inc., Pittsburgh, P.A., 2005.

[31] S. Radhakrishnan, R. Parthsarathi, V. Subramanian and N. Somnathan, Comput. Mater. Sci., 37 (2006) 318. http://dx.doi.org/10.1016/j.commatsci.2005.08.009

[32] M.E. Casida and D.P. Chong (Eds.), Recent Developments in Density Functional Theory, vol. 1, World Scientific, Singapore (1995) pp. 155.

[33] M.E. Casida, K.C. Casida and D.R. Salahub, Int. J. Quantum Chem., 70 (1998) 933. http://dx.doi.org/10.1002/(SICI)1097-461X(1998)70:4

[34] G.A. Guirgis, P. Klaboe, S. Shen, D.L. Powell, A. Gruodis, V. Aleksa, C.J. Nielsen, J. Tao, C. Zheng and J.R. Durig, J. Raman Spectrosc., 34 (2003) 322. http://dx.doi.org/10.1002/jrs.989

[35] P.L. Polavarapu, J. Phys. Chem., 94 (1990) 8106. http://dx.doi.org/10.1021/j100384a024

[36] H. Yoshida, K. Takeda, J. Okamura, A. Ehara and H. Matsurra, J. Phys. Chem. A 106 (2002) 3580. http://dx.doi.org/10.1021/jp013084m

[37] N.B. Colthup, L.H. Daly and S.E. Wiberley, Introduction to Infrared and Raman Spectroscopy, Academic Press, New York, 1990.

[38] J.P. Abraham, Spectrochim. Acta A, 71 (2008) 355. http://dx.doi.org/10.1016/j.saa.2008.01.010

[39] S.N. Terekhov, V.S. Chirvonyi, P.Y. Turpin, J. Appl. Spectrosc., 67(5) (2006) 796. http://dx.doi.org/10.1023/A:1004199313485

[40] D. Sajan, J. Binoy, B. Pradeep, K. Venkata Krishna, V.B. Kartha, I. Hubart Joe and V.S. Jaykumar, Spectrochim. Acta A, 60 (2004) 173. http://dx.doi.org/10.1016/S1386-1425(03)00193-8

[41] K. Furic, V. Muhacek and M. Bonifacic, I. Stefanic, J. Mol. Struct., 267 (1992) 39. http://dx.doi.org/10.1016/0022-2860(92)87006-H

[42] V.K. Rastogi, M.A. Palafox, R.P. Tanwar and L. Mittal, Spectrochim. Acta A, 58(9) (2002) 1987. http://dx.doi.org/10.1016/S1386-1425(01)00650-3

[43] M. Silverstein, G.C. Basseler and C. Morill, Spectrometric Identification of Organic Compounds, Wiley, New York, 1981.